

See discussions, stats, and author profiles for this publication at: <https://www.researchgate.net/publication/323670261>

An object-oriented computational model to study cardiopulmonary hemodynamic interactions in humans

Article in *Computer Methods and Programs in Biomedicine* · March 2018

DOI: 10.1016/j.cmpb.2018.03.008

CITATIONS

11

READS

2,089

5 authors, including:



Chuong Ngo

RWTH Aachen University

41 PUBLICATIONS 168 CITATIONS

[SEE PROFILE](#)



Stephan Dahlmanns

RWTH Aachen University

7 PUBLICATIONS 14 CITATIONS

[SEE PROFILE](#)



Thomas Vollmer

Philips Germany Aachen

21 PUBLICATIONS 111 CITATIONS

[SEE PROFILE](#)



Steffen Leonhardt

RWTH Aachen University

725 PUBLICATIONS 8,867 CITATIONS

[SEE PROFILE](#)

Some of the authors of this publication are also working on these related projects:



BMBF IMEDALytics [View project](#)



Biokybernetik (engl. bio-automation, русский: биокибернетика, 中文: 生物控制论) [View project](#)

An object-oriented computational model to study cardiopulmonary hemodynamic interactions in humans

Chuong Ngo¹, Stephan Dahlmanns¹, Thomas Vollmer², Berno Misgeld¹, Steffen Leonhardt¹

Abstract

Background and Objective

This work introduces an object-oriented computational model to study cardiopulmonary interactions in humans.

Methods

Modeling was performed in object-oriented programming language Matlab Simscape, where model components are connected with each other through physical connections. Constitutive and phenomenological equations of model elements are implemented based on their non-linear pressure-volume or pressure-flow relationship. The model includes more than 30 physiological compartments, which belong either to the cardiovascular or respiratory system. The model considers non-linear behaviors of veins, pulmonary capillaries, collapsible airways, alveoli, and the chest wall. Model parameters were derived based on literature values. Model validation was performed by comparing simulation results with clinical and animal data reported in literature.

Results

The model is able to provide quantitative values of alveolar, pleural, interstitial, aortic and ventricular pressures, as well as heart and lung volumes during spontaneous breathing and mechanical ventilation. Results of baseline simulation demonstrate the consistency of the assigned parameters. Simulation results during mechanical ventilation with PEEP trials can be directly compared with animal and clinical data given in literature.

Conclusions

Object-oriented programming languages can be used to model interconnected systems including model non-linearities. The model provides a useful tool to investigate cardiopulmonary activity during spontaneous breathing and mechanical ventilation.

Keywords: Physiological modeling, object-oriented modeling, cardiopulmonary interactions, non-linear modeling, mechanical ventilation, stroke volume

1. Introduction

1.1. Cardiopulmonary interactions

Cardiopulmonary interactions (CPIs) induced by mechanical ventilation have been studied over the last 50 years based on animal trials and patient data but are still only partly understood [1, 2]. Mechanical ventilation can alter pressure relations within the thorax and can have a beneficial or detrimental effect on the cardiovascular system (CVS) [2]. Clinically relevant aspects have been examined, such as changes in venous return and stroke volume (SV) with positive-pressure ventilation [3, 4, 5, 6].

During spontaneous inspiration, the contraction of respiratory muscles causes a driving force which is transmitted into the pleural space. A fall of the pleural pressure P_{pl} to a more negative value produces a shift in blood volume from the systemic to pulmonary circulation. Accordingly, a rise occurs in the right ventricular SV and a fall occurs in the left one, resulting in a decrease in aortic pressure [7, 8, 9, 10, 11]. The effects of positive-pressure ventilation are inverse. A positive end-expiratory pressure (PEEP) increases the intrathoracic (or pleural) pressure (ITP or P_{pl}), which causes a decreased venous return and a decrease in left ventricular volume [5]. The rise of ITP enlarges the preload and reduces the afterload of the left ventricle; therefore, an improved performance of the left ventricle is expected at the beginning of ventilation with positive pressure [8]. After several heart beats, the cardiac output falls again, which reduces the preload on the systemic side [5, 2].

¹Philips Chair of Medical Information Technology, Helmholtz Institute for Biomedical Engineering, RWTH Aachen University, Pauwelsstr. 20, 52074 Aachen, Germany

²Philips Technologie GmbH Innovative Technologies, Aachen, Germany, Pauwelsstr. 17, 52074 Aachen, Germany

Though the physiological correlations between those parameters have been studied adequately, there is a lack of computational tools which are able to predict the system behavior quantitatively. The aim of this work is to develop a computer model for that purpose.

1.2. Computer-based modeling of CPIs

After Grodins first introduced a dynamic model of the human CVS in 1959 [12], various mathematical models of the CVS have been developed according to the underlying topics [13, 14, 15, 16, 17, 18, 19]. Similarly, modeling of the respiratory system (RS) has been investigated by different groups, ranging from the first order lung model consisting of a resistance and a compliance to multi-compartment models [20, 21, 22, 23, 24, 25]. Rideout's work on computer modeling produced a sophisticated model of human physiology implemented in Fortran [22]. Later, Lu et al. introduced a model applied to analysis of the Valsalva maneuver [26]. In 2009, Jallon et al. introduced a model of the CPS in which the respiratory muscles were modeled by a central pattern generator [9]. In 2016, the group of Chbat et al. developed a model of the CPS that emphasized the interaction of CVS and RS via thorax pressure and gas exchange [23, 27]. These authors followed the compartmental modeling approach with lumped elements, where physical quantities are described by ordinary differential equations. Although these models have succeeded in modeling the circulation system and CPIs, their respiratory model seems to have limitations regarding simplification of the highly non-linear lung with linear elements. Moreover, the models were implemented in signal-based programming languages which do not consider bidirectional flows of energy between the components. Object-oriented modeling languages (OoML), such as Matlab Simscape, Dymola, or Modelica have been shown to provide alternative modeling tools for physiological systems [28, 17]. In this paper, we use OoML to develop a model for studying CPIs in humans.

1.3. Novelty of the model

This paper introduces: (1) the first object-oriented non-linear model of the respiratory system and (2) a new concept of interconnecting the respiratory and the cardiovascular systems via physical connections available in OoML. The model is validated by qualitatively and quantitatively comparing the simulation results with data published in literature. While Jallon's model is limited to spontaneous breathing [9], Albanese/Cheng's model focuses on gas exchange [23, 27], and Lu's model has been validated for the Valsalva maneuver [26], our model is the first one to investigate cardiopulmonary interactions during mechanical ventilation and PEEP trials.

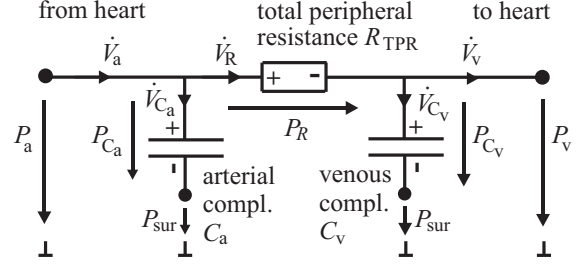


Figure 1: A simple model of a vascular system.

2. Methods

2.1. Object-oriented model

The model is an object-oriented compartment model implemented in Matlab Simscape (sometimes also called "acausal modeling" [28]). In Simscape, physical quantities are modeled with lumped elements, i.e. sources, storages, transformers, converters, sinks, etc. Three types of basic equations can be distinguished: balance, constitutive, and phenomenological equations [29]. Balance equations describe the energy inflow, outflow and storage of a system, or between systems. Constitutive equations (or physical state equations) present the mathematical relation between an across-variable (measured between two terminals: potential, voltage, pressure) and a through-variable (measured at one terminal: flow, current) of one-port or two-port systems [29]. In other words, constitutive equations characterize the energy flow between two potentials, and phenomenological equations describe the sinks and losses of energy by dissipative elements.

In our model, each element is modeled by one or more constitutive equations (pressure-volume characteristics for compliances) or phenomenological equations (pressure-flow characteristics for resistance). Elements are connected with each other via physical quantities including units, which can be written in balance equations. A representative example is the vascular system presented in Fig. 1, which is based on the Windkessel model [30]. Blood flows from the arterial compartment C_a to the venous one C_v through the total peripheral resistance of the vascular bed R_{TPR} . P_a , P_v are the arterial and venous pressure, respectively, and P_{sur} the pressure surrounding the vessel. The balance equations can be written as follows:

$$\begin{aligned}\dot{V}_a(t) &= \dot{V}_{C_a}(t) + \dot{V}_R(t) \\ \dot{V}_R(t) &= \dot{V}_{C_v}(t) + \dot{V}_v(t) \\ P_a(t) &= P_{C_a}(t) + P_{sur}(t) = P_R(t) + P_v(t) \\ P_v(t) &= P_{C_v}(t) + P_{sur}(t)\end{aligned}$$

The constitutive equations presenting the pressure-volume relation of the compliances C_a and C_v :

$$\Delta P_{C_{a,v}}(t) = \frac{1}{C_{a,v}} \cdot \Delta V_{C_{a,v}}(t),$$

and the phenomenological equation for the flow resistance R_{TPR}

$$P_R = \dot{V}_R \cdot R_{TPR} \quad (1)$$

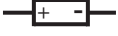
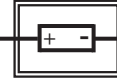


	Linear	Non-linear
resistance R	 $P = R \cdot V$	 $P = f(V)$
compliance C	 $\Delta P = \Delta V / C$	 $\Delta P = g(\Delta V)$

Figure 2: Linear and non-linear customized elements.

are characteristic for these elements. In signal-based or text-based programming languages, an explicit implementation of the balance equations is necessary. In Simscape,¹⁵⁵ because the graphical implementation implies them in the model structure, no explicit implementation is required. Thus, volume and pressure balance equations (1) can be directly derived from Fig.1.

An electrical equivalent representation can be found by¹⁶⁰ replacing hydraulic elements by electrical ones, since pressure, volume, and flow correspond to voltage, charge, and current in the hydraulic-electrical analogy, respectively. This simplification assumes a perfect Newtonian fluid, e.g. constant density and viscoelasticity, within a medium. Moreover, besides the linear elements in the standard library of Simscape, users can create a customized (non-linear) library by implementing the associated constitutive or phenomenological equations of each element (Fig. 2). The double borders in Fig. 2 indicate components with a non-linear behavior.

Our model includes two interconnected parts: the CVS (heart plus pulmonary/systemic circulation) and the RS. The overall system is illustrated in Fig. 3. The model includes more than 30 components.

2.2. Cardiovascular system (CVS)

The cardiovascular model was developed based on the original works of Smith et al. [31, 32]. While the structure of the heart and pulmonary/systemic circulation was preserved, several extensions to the original model have been made. First, the atria were added to the model. Second, it was necessary to include the non-linear behaviors of the pulmonary and systemic veins, as well as the pulmonary capillary resistance and compliance.

2.2.1. Atria and ventricles

Atria and ventricles are elastic elements with an active driving force. Their pressure-volume (PV) relationships were modeled with regard to the end-diastolic pressure-volume relationship (EDPVR) and end-systolic pressure-volume relationship (ESPVR) [15, 17, 32], which are given as

$$P_{es} = E_{es} \cdot (V - V_d) \quad (2)$$

$$P_{ed} = P_0 \cdot (e^{\lambda(V-V_0)} - 1), \quad (3)$$

where E_{es} is the elastance during systole and V_d its filling volume of the ESPVR at zero pressure. P_0 defines the minimal diastolic pressure, λ the curvature of the EDPVR curve and V_0 atrium volume at zero pressure. Eq. 2 and 3 give the systematic behavior for the four heart chambers. The parameters are given in AppendixB with the indexes la, ra, lvf, rvf. Cardiac activity was modeled by activating either eq. (2) or eq. (3) with regard to heart phases. A time-variant driver function $e(t)$ is used to control the transition between the systolic and diastolic pressure:

$$P(V, t) = e(t) \cdot P_{es}(V, t) + (1 - e(t)) \cdot P_{ed}(V, t) \quad (4)$$

The driver function $e(t)$ can be seen as the "pacemaker" of the CVS. According to [32], $e(t)$ can be given by a Gauss distribution (for atria) or sum of four different Gauss distributions (for ventricles and septum). Ventricular and atrial driver functions used in this manuscript are taken from [15]. Detailed parameter for the driver functions are given in AppendixB.

2.2.2. Septum and pericardium

Ventricular interaction is caused by the septum and pericardium. Smith et al. [32] suggested a separation of the ventricles into three components: left ventricle free wall (lvf), septum (spt), and right ventricle free wall (rvf). Each free wall component represents the part of the ventricles which has no influence on the other parts. The septal volume is associated with the inter-ventricular pressure gradient. Septal motion is characterized by a leftward shift towards the left ventricle during systole, and a rightward shift towards the right ventricle during diastole.

The pericardium is a double-walled sac which separates the heart and pleural space. The pericardium volume (V_{pcd}) is, thus, the sum of the ventricular and atrial volumes. Smith et al. [32] simulated the pericardium with one compliance. Its negative pole, corresponding to the outside of the pericardium, matches the pleural pressure P_{pl} . Its positive pole, corresponding to the inside of the pericardium, is connected to all atria and ventricles.

2.2.3. Vascular arteries and veins

The vascular system is a network of a considerable number of blood vessels. To reduce complexity, its function rather than its anatomical structure is often preferred [26, 9, 32, 33]. Applying the Windkessel model to the systemic and pulmonary circulation, allows to determine realistic values of cardiac preload and afterload [32]. In our model, the parameters of the aorta and systemic arteries are simplified to be linear and are adapted from [28].

In contrast, there is more evidence of non-linear characteristics for the veins [31, 34, 35, 36, 37, 38, 39, 40]. According Hainsworth [34] and Rothe [41], the pressure-volume (PV) characteristics of the veins can be divided

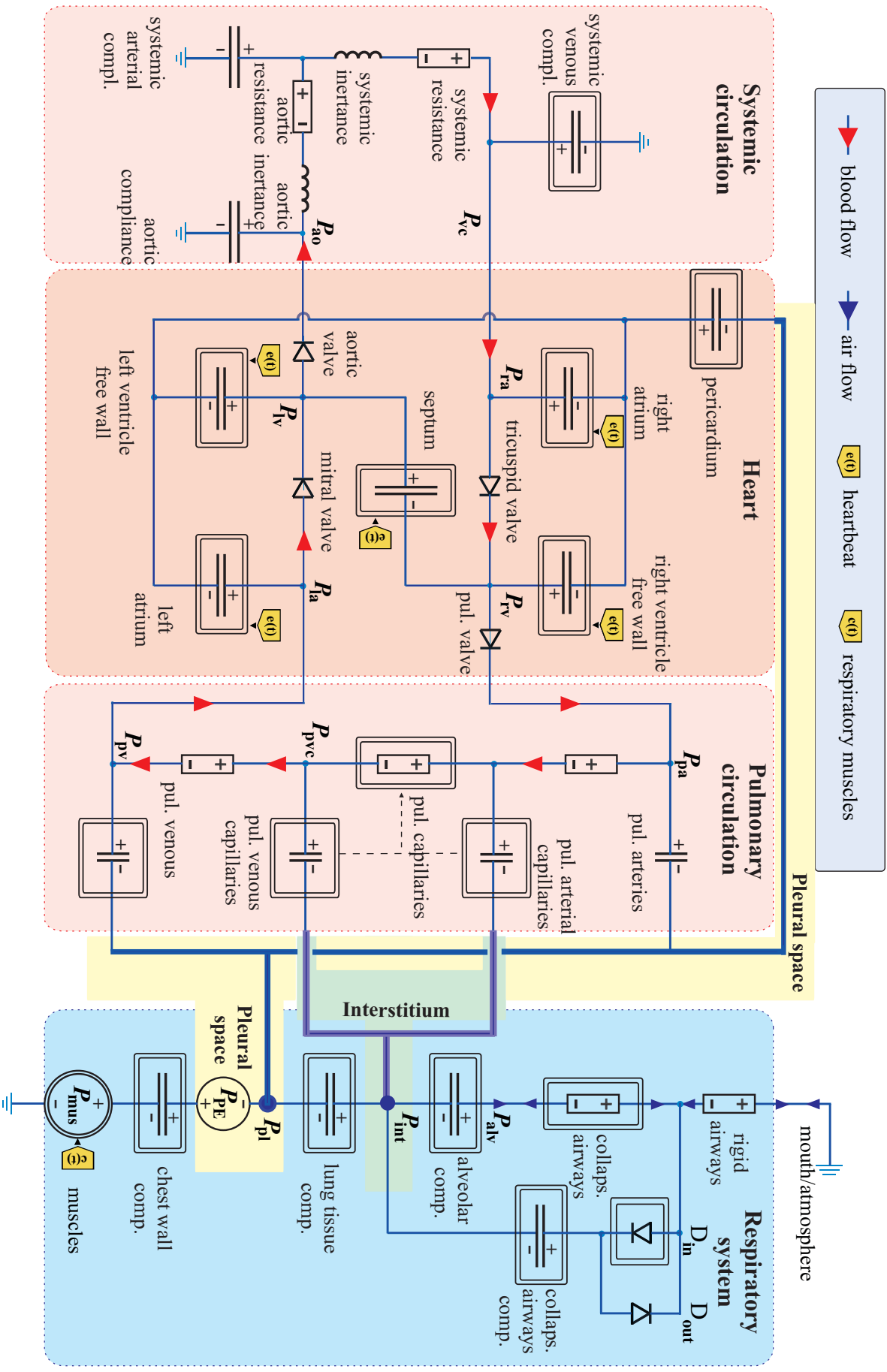


Figure 3: The comprehensive cardiopulmonary model, consisting of the heart, the systemic and pulmonary circulation, and the respiratory system. Flows are distinguished between blood flow (red arrows) and air flow (blue arrows). pul. = pulmonary; comp. = compliance. List of indexes is given in Appendix A.

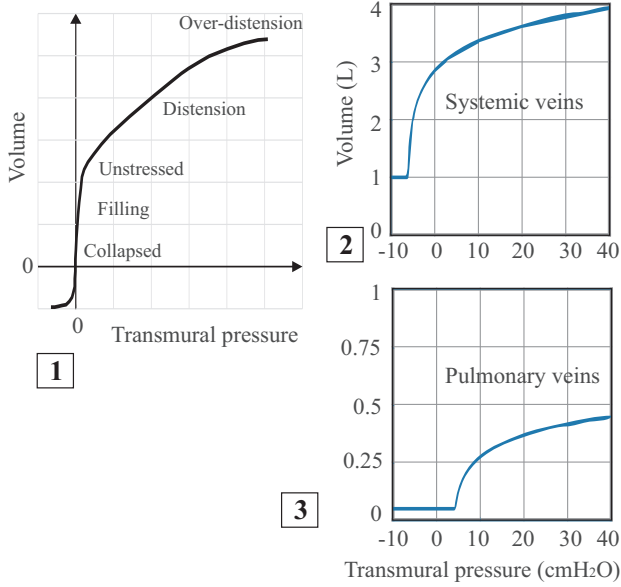


Figure 4: (1) Pressure-volume (PV) characteristics of a collapsible tube, reproduced from [34]. (2) PV relation of the systemic veins. (3) PV relation of the pulmonary vein.

into over-distension, distension, filling, and collapsed condition (see Fig. 4). Such a behavior can be modeled by a log function:

$$V = \frac{1}{\lambda} \cdot \log(P_{tm} + P_0) + V_0. \quad (5)$$

V is the volume, P_{tm} is the transmural pressure, P_0 , V_0 and λ are three parameters of the log function. This function has a very high gradient at the beginning which changes quickly to a lower one after a certain point. In our model, these parameters are calculated by assuming approx. 3 L blood volume in the systemic veins and 300 mL blood volume in the pulmonary veins at normal blood pressures. Figure 4 presents the characteristics of the implemented systemic and pulmonary veins.

Unlike the separated vessel, the systemic and pulmonary veins are networks of vessels tethered to the surrounding tissues which prevent them from a total collapse at low transmural pressures. This means that the venous compartment must maintain a nonzero volume even at zero or negative pressure, as observed in animal experiments [42, 34, 41]. For simplification, we considered a minimum volume of 1 L for the systemic veins. Under normal conditions, venous pressure remains slightly positive and the systemic volume is around 3 L.

2.2.4. Lung capillaries

The lung capillaries are located directly around the lung alveoli within the tissue and play an important role in CPIs. In our model, a hyperbolic PV relationship

$$V(t) = V_0 + \frac{1}{\lambda} \cdot \tanh(c \cdot P_{tm}(t) + P_0) \quad (6)$$

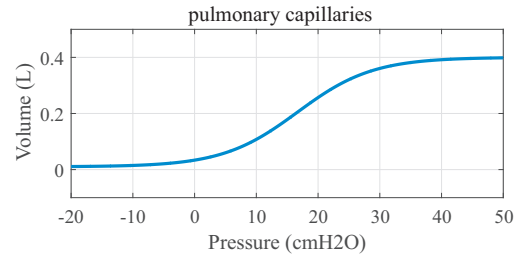


Figure 5: PV-characteristics of lung capillaries

was applied for the lung capillaries. V_0 , c , and P_0 are constant parameters. Their values were determined based on following physiological considerations [39, 40]:

1. The transmural pressure $P_{tm}(t)$ of lung capillaries in a healthy body is $P_{tm} \approx 15 \text{ cmH}_2\text{O}$ ($= P_{cap} - P_{int} = 10 - (-5) \text{ cmH}_2\text{O}$), P_{cap} is the pressure in the lung capillaries and P_{int} the interstitial pressure.
2. At this pressure, total blood volume within the lungs is approx. 200 mL.
3. At normal transmural pressure, the PV relationship can be considered as linear and described by an ideal capacitor.
4. At immoderately low pressure, the capillaries collapse to a minimum volume of approx. $V_{min} = 10 \text{ mL}$.
5. The maximum volume of lung capillaries is assumed to be 400 mL. If this value is achieved, all lung capillaries are recruited.

For a detailed description of the CPIs, the capillary compliance was divided into pulmonary arterial and pulmonary venous capillary components (Fig.3), which simulates the total PV characteristics shown in Fig. 5.

Flow resistance of the lungs capillaries $R(t)$ is inversely proportional to the square of their filling volume $V(t)$ according to the law of Poiseuille:

$$R(t) = R_1 \cdot \frac{(V_1 - 0.9V_{min})^2}{(V(t) - 0.9V_{min})^2}. \quad (7)$$

V_1 and R_1 are resistance and volume at normal transmural pressure. V_{min} is the minimal volume of capillaries during collapse. Table 1 presents the parameters for the pulmonary capillaries. Its flow resistance is equal to $69.75 \text{ cmH}_2\text{OL}^{-1} \text{ s}$ at a filling volume $V = 200 \text{ mL}$, and reaches the maximum value $R = 2.5 \cdot 10^6 \text{ cmH}_2\text{OL}^{-1} \text{ s}$ at the collapsing volume $V = V_{min} = 10 \text{ mL}$.

2.3. The respiratory system (RS)

In the 1950s, Otis et al. [20, 43] modeled the human RS as a series of resistance R and compliance C (passive elements), which are driven by the respiratory muscles in the form of a sinusoidal pressure source (active element). Although this simplification has been used until modern times [24, 9], lung mechanics are actually highly

Table 1: Parameters of the pulmonary capillaries. V_1 , V_0 , and V_{min} are given in L, R_1 in $\text{cmH}_2\text{O L}^{-1} \text{s}$, and λ in L^{-1} . c is a scalar.

Resistance		Compliance	
Parameter	Value	Parameter	Value
V_1	0.2	V_0	0.1025
R_1	70.8725	P_0	-1.3687
V_{min}	0.005	λ	10.256
		c	0.0821

non-linear, especially in the presence of lung pathologies. Our RS model is based on the basic assumptions and extensions of Liu et al. [44] and Athanasiades et al. [45], which focused on non-linearities of lung parameters. Our RS model can be divided into seven main compartments: respiratory muscles, pleural space, chest wall, lung tissue, alveoli, and the non-collapsible and collapsible airways.

2.3.1. Respiratory muscles

The respiratory muscles, consisting of the diaphragm and the intercostal muscles, contract during inspiration and release during expiration. They are modeled by a pressure source which connects the chest wall C_{cw} and the atmosphere at body surface. The alignment of the pressure source in the circuit indicates a negative P_{mus} . During inspiration, P_{mus} and the pleural pressure P_{pl} become more negative, which drives air into the alveoli. The gas volume entering the lungs ΔV_L is equal to the volume change of the thorax ΔV_{cw} . Experimental data have shown an exponential form of pleural pressure P_{pl} in healthy subjects [40], which indicates an exponential characteristic curve of P_{mus} . The implementation of P_{mus} is presented in AppendixD.

2.3.2. Chest wall and pleural space

The chest wall compliance C_{cw} provides the elasticity of the components surrounding the lungs, i.e. thorax and diaphragm. According to Athanasiades et al. [45], the non-linear pressure-volume curve of C_{cw} is sigmoidal and can be modeled by

$$P_{cw}(t) = A_{cw} - B_{cw} \cdot \log\left(\frac{TLC - RV}{V_{cw}(t) - RV} - 0.999\right). \quad (8)$$

The chest wall compliance C_{cw} is the quotient of volume change over pressure drop and can be calculated as

$$C_{cw}(t) = \frac{TLC - RV}{B_{cw}} \cdot \frac{\exp\left(\frac{A_{cw} - P_{cw}(t)}{B_{cw}}\right)}{\left[\exp\left(\frac{A_{cw} - P_{cw}(t)}{B_{cw}}\right) + 0.999\right]^2}, \quad (9)$$

where TLC is the total lung capacity, RV is the lung residual volume, and A_{cw} and B_{cw} are constants. Taking parameters from [45] will result in a maximum chest wall compliance of $0.3 \text{ L/cmH}_2\text{O}$, compared with the average value of $0.2 \text{ L/cmH}_2\text{O}$ [39, 40, 46].

The parameter A_{cw} from [45] causes a pressure drop over the chest wall $P_{cw} = 0 \text{ cmH}_2\text{O}$ and a pleural pressure $P_{pl} = 0 \text{ cmH}_2\text{O}$ at normal filling volume of the lungs. Indeed, in normal condition, a negative pleural pressure $P_{pl} \approx -5 \text{ cmH}_2\text{O}$ prevails for a normal lung volume of 3 L [39]. Thus, models which use two compliances in series fail to present the negative pleural pressure. To overcome this problem, we introduced the extended pleural pressure source P_{PE} in our previous works [47, 48]. P_{PE} incorporates the pre-stress of the chest walls and lung tissue, so that the lungs are stretched and the chest wall is shrunk at functional residual capacity (FRC). The pressure gradient between chest wall and lung tissue should be around $10 \text{ cmH}_2\text{O}$ [40] and can be realized by a choice of $P_{PE} = 10 \text{ cmH}_2\text{O}$. This pleural-extended model succeeds in not only presenting the well-known PV characteristics of the chest (Fig. 6), but also the negative pleural pressure $P_{pl} \approx -5 \text{ cmH}_2\text{O}$. With the introduction of P_{PE} , A_{cw} needed to be adapted to achieve the original chest compliance curve (Fig. 6). The parameters of the chest wall and pleural space are given in Table 2.

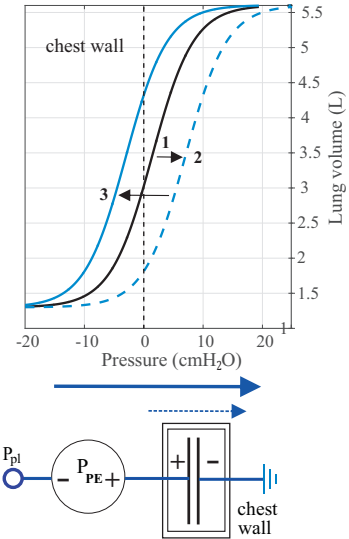


Figure 6: Implemented chest wall compliance according to [45]: (1) is the original curve; (2) is the curve after adaption of A_{cw} , and (3) after adaption of P_{PE} . P_{pl} is negative at lung volume $< 4.25 \text{ L}$.

Parameter	Value	Unit
TLC	5.6	L
RV	1.3	L
A_{cw}	7	cmH_2O
B_{cw}	3.5	cmH_2O
P_{PE}	10	cmH_2O

Table 2: Parameters of the chest wall and pleural space.

2.3.3. Lung tissue

Recent models of respiratory mechanics consider the elasticity of the lungs as one compartment [44, 45, 26, 49, 24, 25], ignoring the physiological distinction between elastic lung tissue and alveoli surface tension based on the theory of balloon stability [50, 51]. The PV characteristics of lung tissue without alveolar impact can be experimentally determined by filling the alveoli with isotonic saline. By reducing the surfactant concentration and, thus, the surface tension, lung compliance increases threefold [39, 52] from 0.2 L/cmH₂O [44, 39] to 0.6 L/cmH₂O. This component, representing the elasticity of the elastic tissue and alveolar wall, must be at least as high as this value and, in the present work, was considered to be constant $C_{\text{tissue}} = 1$ L/cmH₂O.

2.3.4. Alveoli

Although the mechanical behavior of alveoli surface tension has been investigated by different groups [50, 53, 54, 55, 56, 57], it is not yet completely understood [58]. In their work, Yuta [55] and Sundaresan et al. [56] assumed that the volume change of the lung during spontaneous breathing is mainly caused by the recruitment of alveoli and not by further expansion of the opened alveoli. Implementation of their work requires a large number of interconnected components. In our approach, we aimed to present the PV characteristics of alveoli through clinical data measured in healthy and diseased subjects. Therefore, we considered the alveoli characteristics as one non-linear component. The PV characteristics of lung alveoli can be described by a hyperbolic function:

$$V(t) = V_0 + \frac{1}{\lambda} \cdot \tanh(c \cdot P(t) + P_0),$$

where the parameters V_0 , λ , c and P_0 can be determined by maximum and minimum lung volume, as well as maximum alveoli compliance. By changing these parameters, the shape of the compliance curve can be adjusted. In Fig. 7, the upper line represents the alveolar compliance curve, and the lower one the compliance of diseased lungs, such as in edematous patients [55]. Parameters used in our simulation are given in Table 3. The black circles in Fig. 7 illustrate residual lung volume (RV = 1.3 L [39]). The minimal volume of 0.5 L corresponds to the state when the lungs are separated from the thorax and are completely collapsed. This approach does not yield any contradiction with the balloon-like theory or the recruitment model [55].

The lung compliance C_L is a series of tissue and alveoli compliances and, in our case, is equal to 0.2308 L/cmH₂O. In practice, C_L can only be measured independently from C_{cw} by using an esophageal catheter [8]. The total respiratory compliance C_{total} , consisting of lungs and chest wall, is thus a series of C_{tissue} , C_{alv} , and C_{cw} :

$$\frac{1}{C_{\text{total}}} = \frac{1}{C_L} + \frac{1}{C_{\text{cw}}} \quad (10)$$

$$= \frac{1}{C_{\text{tissue}}} + \frac{1}{C_{\text{alv}}} + \frac{1}{C_{\text{cw}}}. \quad (11)$$

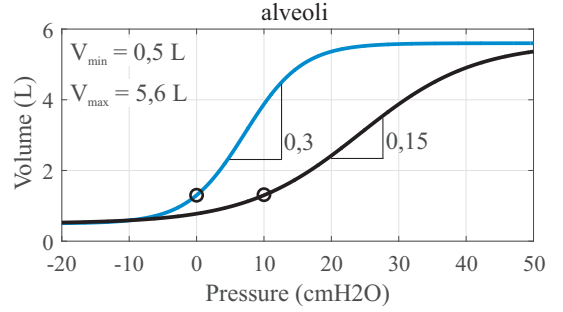


Figure 7: Alveolar compliance for healthy (blue) and edematous lungs (black). Maximal compliance is equal to 0.3 L/cmH₂O for healthy lungs and up to 0.15 L/cmH₂O for diseased lungs. Circles mark residual lung volume.

Parameter	Value	Unit
V_0	3.05	L
λ	0.3922	L ⁻¹
c	0.1176	-
P_0	-0.8409	cmH ₂ O

Table 3: Parameters of the alveoli compartment.

2.3.5. Airways

Airway resistance was divided into rigid and collapsible resistances (R_{rig} and R_{col} , respectively). Physiologically, the rigid part of the airway system consists of mouth, glottis, and trachea, while collapsible resistance presents the remaining part of the bronchial tree. In our model, a constant rigid resistance $R_{\text{rig}} = 1 \text{ cmH}_2\text{O L}^{-1} \text{ s}$ was assumed, which is approximately 25 % of the total resistance [39].

The collapsible resistance R_{col} is inversely proportional to the bronchial and the lung volume [59] and can be given as follows:

$$R_{\text{col}}(t) = R_1 \cdot \frac{V_1 - 0.9V_{\text{min}}}{V_{\text{col}}(t) - 0.9V_{\text{min}}}, \quad (12)$$

where $V_{\text{col}}(t)$ is the volume of the collapsible airways while R_1 , V_1 , and V_{min} are constants. The PV curve exhibits a similar behavior to that of the cardiovascular veins, which can be written by a logarithmic function [31, 35, 60, 36]:

$$V_{\text{col}}(t) = \frac{1}{\lambda} \cdot \ln(P_{\text{col}}(t) + P_0) + V_0, \quad (13)$$

where $P_{\text{col}}(t)$ is the transmural pressure drop between inner and outer wall of the collapsible airways. The parameters V_0 , P_0 , and λ are given in Table 4. The cumulative volume of the collapsible airways is estimated to be about 50 mL. At this volume, the collapsible resistance is approx. 75 % of the total resistance [39]. When a bronchial airway collapses, the fluid film within the inner wall of the bronchi

becomes a closed fluid layer, which causes the bronchial to stick together. To reverse this process, i.e. open the bronchi, a higher pressure is necessary to overcome the surface tension of the new fluid layer [61, 62]. Chen et al. [62] estimated the opening pressure P_{open} at 5 cmH₂O at different levels of P_{pl} . This phenomenon was implemented in our model by connecting the airway compliance C_{col} in series with two diodes D_{in} and D_{out} (an electrical form of hydraulic valve). A positive flow through D_{in} increases airway volume V_{col} and vice versa. If V_{col} drops below a threshold value, the opening pressure (breakdown voltage of an electrical diode) of D_{in} increases. Fig. 8 shows the model structure and the PV-characteristics of the collapsible airways.

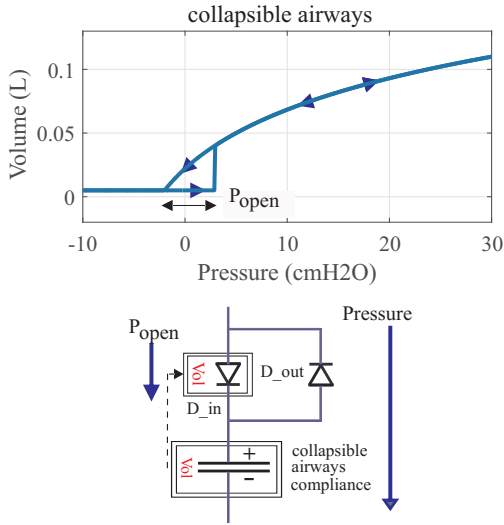


Figure 8: Pressure-volume characteristics of the collapsible airways. A higher pressure is needed to open the collapsed airways.

Resistance		Compliance	
	Value	Parameter	Value
V_1	0.05	V_0	-0.0872
R_1	3	P_0	7.4414
V_{min}	0.005	λ	18.3776
		P_{open}	5

Table 4: Parameters of the collapsible airways

2.4. Model Implementation in Simscape

In signal-based or text-based programming languages, an explicit implementation of the balance equations would be necessary (see [23]). In object-oriented Simscape, the graphical implementation of the model structure implies these equations, hence, no explicit equations for the 'connection' of components are needed. The main Simscape program consists of the same blocks as shown in Fig. 3.

The implemented cardiovascular model (Fig. 3) consists of the heart and the pulmonary/systemic circulation. Non-

linear resistances and capacitors were developed as Simscape elements according to the mathematical equations presented above. The positive pole of the ventricle-free wall is connected to the heart valve. A flow at that pole corresponds to the filling of the heart with blood, while a flow at the negative pole of the ventricle describes a volume replacement of the thorax through the heart, which is coupled to the pericardium and eventually, the pleural space.

The parameters of the heart components are given in Appendix B and Appendix C. The heart valves were modeled with ideal diodes with a transmitting pressure of 10^{-5} cmH₂O, a blocking resistance of 10^5 cmH₂O s L⁻¹, and various transmitting resistances (Table B.12).

Components	Param.	Value
aortic compliance	C_{ao}	0.000168
syst. arteries compliance	$C_{\text{sys,art}}$	0.0011
aortic resistance	R_{ao}	91.78
syst. resistance	R_{sys}	1359.5
aortic inertance	L_{ao}	1.1216
syst. inertance	L_{sys}	4894.4
pul. art. resistance	R_{pa}	94.5
pul. art. compliance	C_{pa}	0.0022
pul. ven. resistance	R_{pv}	31.5

Table 5: Parameters of systemic and pulmonary circulation, from [31, 28]; resistances are given in [cmH₂O L⁻¹ s], compliances in [L cmH₂O⁻¹], and inertances in [cmH₂O L⁻¹ s²].

Table 5 summarizes the linear parameters of the systemic and pulmonary circulation according to Fig. 3. All compliances in the model have an initial volume which is set at the beginning of the simulation. The systemic veins are filled with 3.1 L, the systemic arteries and capillaries with 600 mL. On the pulmonary side, initial volume is set to 100 mL for the arteries, 100 mL for the capillaries, and 50 mL for the veins. Both heart ventricles have an initial volume of 40 mL.

The RS is implemented by connecting its six functional compartments, as shown in Fig. 3. At the airway opening, the model is connected to a reference atmospheric pressure P_{atm} , or to a ventilator in case of mechanical ventilation. The interstitial pressure occurs at the negative pole of the alveolar and the positive pole of the tissue compartment, while the pleural pressure separates lung tissue from the chest wall. Each compliance has the functionality of a physiological barrier between two different media. At the beginning of the simulation, several initial values have to be set to achieve realistic results. Alveolar and chest wall volumes were set to 1.8 L.

CVS and RS were mechanically coupled by the pleural pressure P_{pl} and interstitial pressure P_{int} . The pericardium, pulmonary arteries and veins are surrounded by P_{pl} , and the pulmonary capillaries by P_{int} . These inter-

actions were implemented in the Simscape model through physical connections between the corresponding elements. The overall system is presented in Fig. 3

Under normal conditions, 20% (approx. 1 L) of the total blood volume is located in the heart and pulmonary circulation [39, 40] within the thoracic cage. The chest wall capacity (V_{cw}) from eq. (8) has to be adapted, since Athanasiades et al. [45] did not consider the thoracic blood volume (TBV) and assumed that the maximal chest wall volume is equal to the total lung capacity (TLC). Thus, $V_{cw,max}$ was increased to $TLC + 1L$, the parameter B_{cw} in eq. (9) was adapted to

$$B_{cw} \approx \frac{V_{max} - RV}{4 \cdot C_{cw,max}} \approx 4.75 \text{ cmH}_2\text{O}. \quad (14)$$

The new parameters of the chest wall are given in Table 6. The initial value of chest wall volume was increased to 2.05L by taking the TBV into consideration.

Parameter	RS only	CPS	Unit
A_{cw}	7	7	cmH ₂ O
B_{cw}	3.5	4.75	cmH ₂ O
V_{max}	5.6	6.6	L
RV	1.3	1.3	L
P_{PE}	10	10	cmH ₂ O

Table 6: Adaptation of the chest wall parameter with regard to thoracic blood volume from the respiratory to cardiopulmonary system.

3. Results

The model was simulated using the backward Euler routine at a fixed step size of 10ms. On a PC with an Intel Core i7-4770 CPU, the simulation speed is approximately 30 times faster than in real time. This section compares the simulation results with human and animal experimental data from literature. Model validation is divided into two part: the baseline simulation and simulation of CPIs.

3.1. Baseline simulation

3.1.1. Cardiovascular pressures and volumes

In this part of the validation, we showed the consistency of the model regarding the assigned parameters for a normal, healthy subject. Each simulation had an initial phase, in which the volumes started to redistribute according to the ratio between the vessels' compliances. The driver functions were activated at $t=20s$ and $t=25s$ for ventricles and atria, respectively. Figure 9 presents the change in systemic arterial volume during the initial phase. The system reached its operating points after approx. 40s. The resulting pressure and volume relations for the simulation of a healthy person are presented in Fig. 10 for three random heart cycles. The aortic pressure rose to 169 cmH₂O (124.3 mmHg) in systole and fell to 110

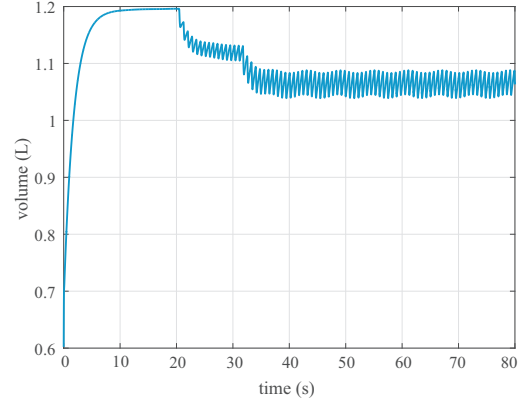


Figure 9: Changes in systemic arterial volume during the initial phase of the simulation. From a start value at 0.6 L, the volume reaches a stationary value of 1.2 L. After the heart started to pump at $t = 20$ s, the volume stabilized at around 1.05-1.09 L.

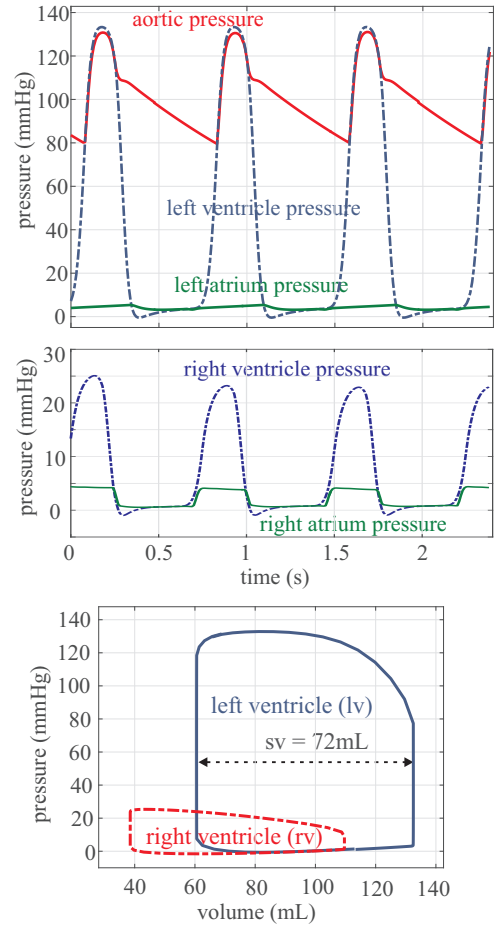


Figure 10: Simulative results of the decoupled CVS. Top two graphs: aortic, left ventricle and left atrium pressure over three heart cycles. Bottom graph: pressure-volume curve of the left and right ventricles.

cmH₂O (80.9 mmHg) in diastole. Stroke volume was equal to 72 mL, which equates to a cardiac output of 5.76 L/min at a heart rate of 80 beats per min.

Table 7 presents the pressures as well as cardiac and stroke indexes compared to the standard range of a healthy

person taken from [63]. Cardiac and stroke indexes were calculated for a total body surface of 1.73 m^2 . All parameters are in physiological normal ranges. The simulated total blood volume was equal to 5 L on average. Table 9 compares blood volume in different compartments between the simulation and data from [39, 40]. Some values found in literature are calculated assuming a total body blood volume of 5L multiplied with the given percentage values. Figure 11 displays the blood distribution for the model compartments.

Parameter	Model	Standard [63]
Pressures (mmHg)		
Left ventricle systolic	124	90 – 140
Left ventricle end-diastolic	6	5 – 12
Left atrial	3.5 – 5	2 – 12
Arterial systolic	122	90 – 140
Arterial diastolic	81	60 – 90
Right ventricle systolic	25	18 – 30
Right ventricle end-diastolic	0.5	-0.5 – 4.5
Right atrial mean	0	-2 – 2
Pulm. artery systolic	26	13 – 30
Pulm. artery diastolic	11	3 – 15
Pulm. capillary wedge max	10 – 16	8 – 23
Pulm. capillary wedge min	6 – 11	5 – 14
Others		
Cardiac index (l/min/m^2)	3.33	2.5 – 5.3
Stroke index (ml/beat/m^2)	41.63	37 – 72

Table 7: Baseline simulation results of pressures, cardiac and stroke indexes. The indexes were calculated with a total body surface of 1.73 m^2 . Standard values are given in [63].

Compartment	Min (mL)	Max (mL)	Mean (mL)
Left atrium	38	45	
Right atrium	35	50	
Left ventricle	60	130	
Right ventricle	48	120	
Heart	181	345	263
Pulmonary arteries	240	290	265
Pulmonary capillaries	170	220	195
Pulmonary veins	289	296	293
Systemic arteries and capillaries	240	290	265
Systemic veins	2820	2920	2870
Total	4757	5189	4973

Table 8: Simulated result of blood volume distribution.

Volume	Model	[39]	[40]
Systemic veins	2820-2920 mL	3200 mL	2700 mL
Pulm. arteries	240-290 mL	70 mL	400 mL
Pulm. veins and capillaries	459-516 mL	450 mL	750 mL

Table 9: Comparison of blood volume between model and data reproduced from [39, 40]. If literature values were given in percentage, calculation was made based on a total blood volume of 5 L.

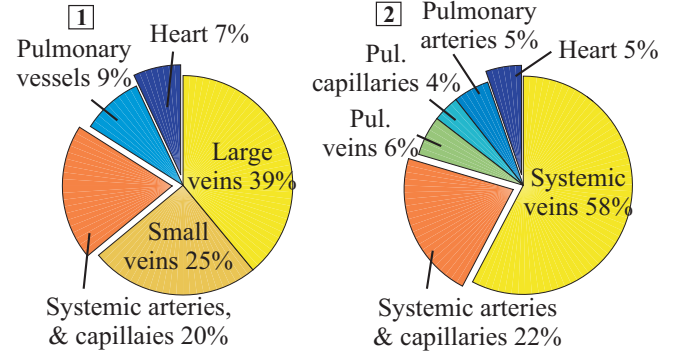


Figure 11: Blood volume distribution of the human body. (1) Literature values, reproduced from [39]. (2) Simulation results. Total blood volume is approx. 5 L.

3.1.2. Dynamic and static behaviors of the RS

A simulation was performed for spontaneous breathing with a respiratory rate of 0.2 Hz (12 breaths/min) and a signal amplitude of $5 \text{ cmH}_2\text{O}$ for P_{mus} . Inspiration and expiration time were set to 2s and 3s, respectively. Figure 12 presents the simulative results of muscles, alveolar, interstitium, and pleural pressure, as well as lung volume, in comparison with data reproduced from [39]. Simulation results correlate well with the literature values.

At end-expiration ($t \approx 45 \text{ s}$), the pleural pressure was $P_{\text{pl}} = -5.74 \text{ cmH}_2\text{O}$, the interstitial pressure $P_{\text{int}} = -4.94 \text{ cmH}_2\text{O}$, and the alveolar pressure $P_{\text{alv}} = 0.015 \text{ cmH}_2\text{O}$. During inspiration, pressures of the whole system decreased below P_{atm} , so that air entered the lungs and loaded the compliances. At the end-inspiratory phase, minimal pressures occurred equal to $P_{\text{int}} = -7.1 \text{ cmH}_2\text{O}$ in the interstitium and $P_{\text{pl}} = -8.3 \text{ cmH}_2\text{O}$ in the pleural space. FRC was equal to 2.5 L, with a tidal volume V_T of 500 mL. All values and dynamics described in [39] can be successfully simulated.

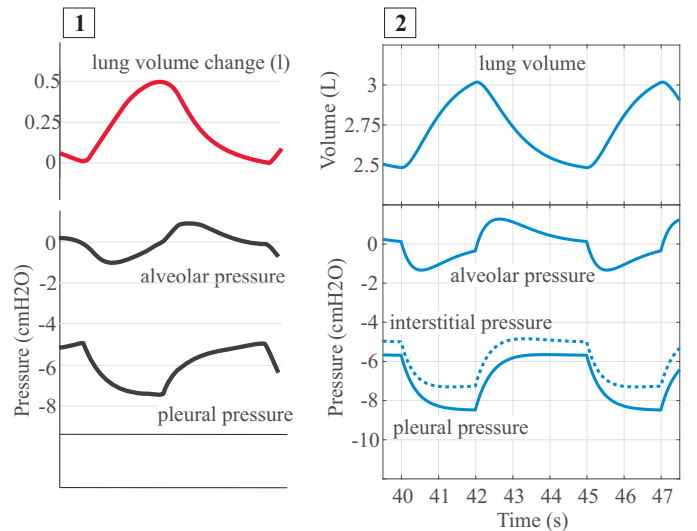


Figure 12: Respiratory pressures and volumes during spontaneous breathing. (1): Literature values, reproduced from [39]. (2) Simulation results with a functional residual capacity of 2.5L.

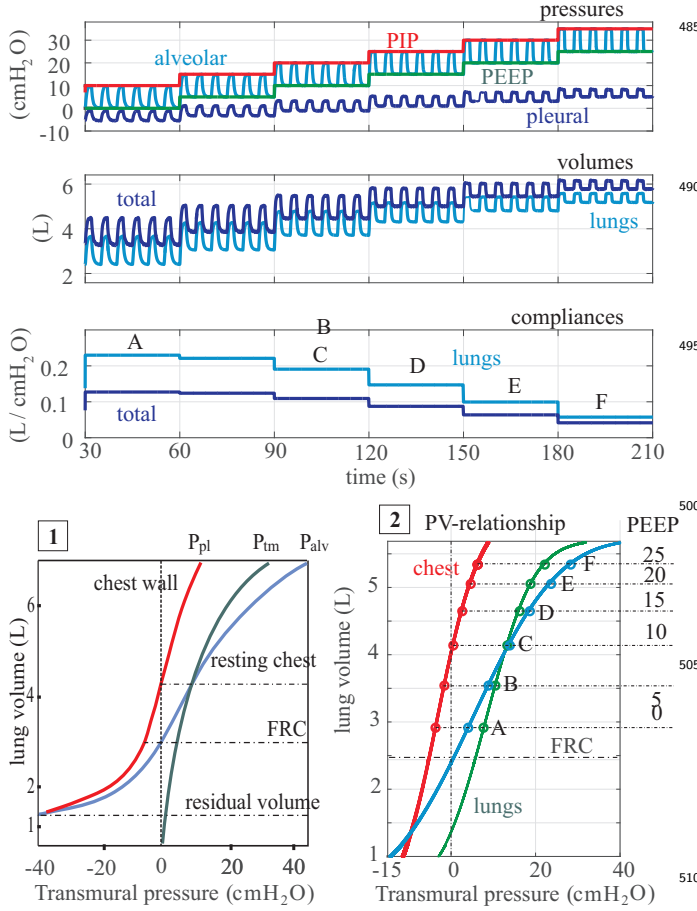


Figure 13: Top three graphs: ventilation pressures, lung volumes and compliances during a PEEP trial. PEEP was incrementally increased from 0 to 25 cmH₂O, PIP was set equal to PEEP + 10 cmH₂O. Non-linear compliance changes with increased PEEP are observed. Bottom graph: Static pressure-volume loop of the modeled lung and chest wall (1): Literature values, reproduced from [40], (2): Simulation results. A-F mark the operating points of the system for each set of PEEP and PIP.

The PV characteristics of the lungs play a key role in patient monitoring during mechanical ventilation. For example, lung over-stretching can occur if airway pressure exceeds 30 cmH₂O [64]. This behavior was modeled by considering the non-linear characteristics of lung and chest wall compliance. To demonstrate non-linear behavior during PEEP-trial, we constructed a model of a ventilator and applied pressure-controlled ventilation (PCV) at the patient's mouth. Incremental increase of positive end-expiratory pressure (PEEP) and peak inspiratory pressure (PIP) allowed us to investigate the dynamic response of lung mechanics to PEEP. The respiratory muscles were deactivated as soon as mechanical ventilation started.

In Fig. 13, the top three panels present the results including alveolar and pleural pressure, lung volume, as well as lung and total compliance. The total respiratory compliance C_{total} was calculated as the quotient of the tidal volume V_T and the overall pressure drop [24]:

$$C_{\text{total}} = \frac{V_T}{\text{PIP} - \text{PEEP}}. \quad (15)$$

From zero, PEEP was incrementally increased by 5 cmH₂O every 30 s. The pressure difference between PIP and PEEP remained at 10 cmH₂O during the entire simulation. P_{pl} rose together with PEEP and became positive at high ventilation pressures ($P_{\text{ven}} > 15$ cmH₂O). From this point, the RS started to reach saturation, and total compliance decreased from 0.124 L/cmH₂O at PEEP = 0 to 0.03 L/cmH₂O at PEEP = 25 cmH₂O. Lung compliance also decreased, causing a large rise in mechanical stress over the lungs, from 5.74 cmH₂O (PEEP = 0) to 20 cmH₂O (PEEP = 25). As a result of this stiffness, tidal volume fell from 1.241 L (PEEP = 0) to 0.272 L (PEEP = 25). The mean pressure and volume of each PEEP setting fit exactly into the static PV-relationship of lung and thorax. Due to the increasing PEEP, the operating point moved upwards from A (PEEP = 0) to F (PEEP = 25) in Fig. 13, bottom panel (2). The simulation results correlates well with the data reconstructed from [40] (bottom panel (1)). The simulation results demonstrate the ability of the model to quantify the non-linear changes in tidal volume and compliance during a PEEP-trial.

3.2. Simulation of CPIs

This validation part presents simulation results of the model under mechanical ventilation compared to clinical or animal studies in literature. It should be noted that the model parameters are assigned regarding unrelated studies and reports. Since these parameters can vary among species, individuals and pathologies, a perfect curve fitting can only be performed by algorithmic parameter estimation. Otherwise, changing values via "try and error" may lead to parameter "manipulation" to fit the data. For that reason, we decided to keep the same parameters of the above mentioned cardiopulmonary system for all following simulations. The only signals that changed are model inputs: muscle or pleural pressures during spontaneous breathing or airway pressure during mechanical ventilation. One exception is a patient with severe lung restriction and will be mentioned explicitly.

3.2.1. Mueller maneuver

During spontaneous inspiration, a fall of P_{pl} causes a shift in blood volume from the systemic to pulmonary circulation, which results in a decrease in aortic pressure. Robotham et al. [65] observed a significant increase in aortic pressure, transmural left and right ventricular filling pressure during the Mueller maneuver in closed-chest, anesthetized, neurally intact Mongrel dogs [65]. We created the scenario by inactivating the respiratory tract due to zero gas flow, and setting the pleural pressure from 0 to -12 cmH₂O and back to 0 within a duration of 8 heart beats, which was the same in the experiment. Transmural pressures were calculated by subtracting the pleural pressure. Figure 14 compares animal data (1) and simulation results (2). Significant points are marked with exact values. The transmural aortic pressure reached its maximum

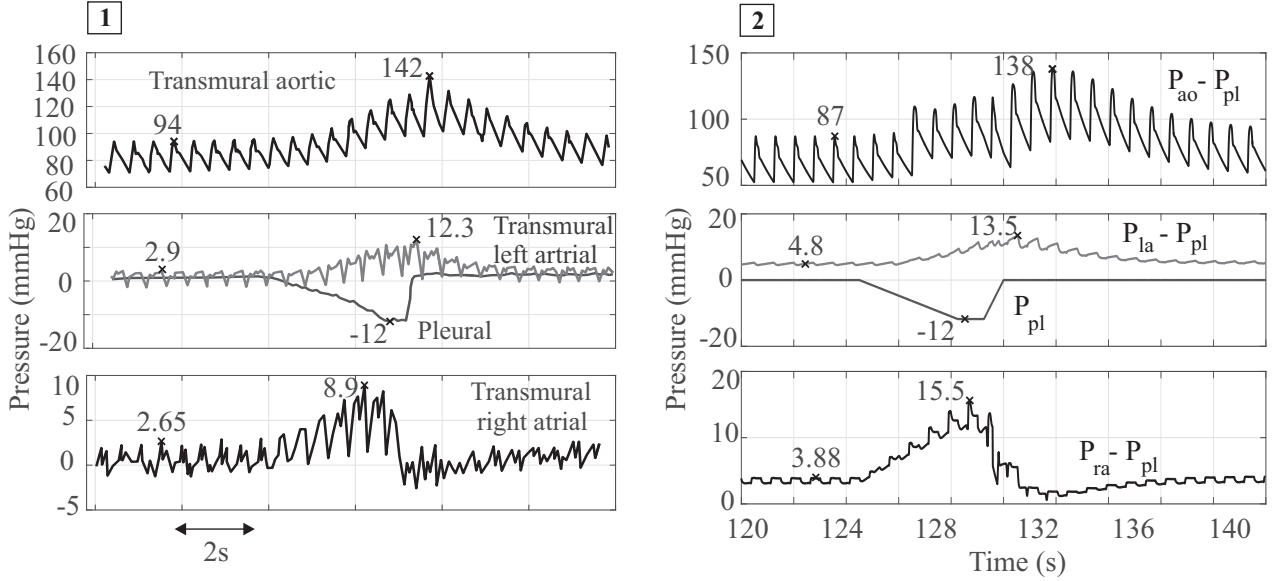


Figure 14: Pressure relations during a Mueller maneuver. The pleural pressure, as well as transmural aortic, left and right atrial pressures are depicted. (1) Data measured on a neurally intact Mongrel dog, reproduced from [10]. (2): Model simulation results. The pleural pressure in the model was set from 0 to -12 cmH₂O and back to 0 within 8 heart beats.

at 138 mmHg (142 mmHg in animal data) at the second heart beat after the end of the maneuver. The transmural right atrial pressure increased during the first 5 heart beats then abruptly fell to a negative value. In total, simulated pressure relations and dynamic behaviors were observed as expected.

3.2.2. Pressure relations during ventilation

To demonstrate the behavior of the model during mechanical ventilation, we constructed a model of the ventilator. First comparison is based on a lung-diseased patient under volume-controlled-ventilation (VCV) reported by Jardin et al. [8].

Electrocardiogram (ECG), airway (A), esophageal (E), right atrial (RA), and pulmonary capillary wedge (PCW) pressures were simultaneously recorded. Tidal volume was 12 ml/kg (840 ml for a 75 kg patient). Peak ventilation pressure was 45 cmH₂O. Fig. 15 shows the comparison of simulation and clinical data. In simulation (2), tidal volume was set to $V_T = 3.2$ L to achieve the peak pressure of 45 cmH₂O. Simulation (3) was performed at $V_T = 840$ mL which resulted in a peak pressure < 10 cmH₂O. The results demonstrate, that such a high pressure at a low tidal volume does not occur in a healthy subject. In fact, this pressure-volume ratio indicates a severe restrictive disease with a dramatic drop in the lung compliance. In simulation (4), we reduced the lung compliance (alveolar and tissue compliance) to 10% of the original values, so that peak pressure of 45 cmH₂O can be achieved at $V_T = 840$ mL. Simulation results predict a possible pathological change in lung compliance which corresponds to the patient's condition.

In the same data, Jardin observed greater increase in the pulmonary capillary wedge pressure (PCW) than in

the esophageal pressure leading to an increased left ventricular volume; and a smaller increase in right atrial than in esophageal pressure, which indicates a decrease in right ventricular volume. This pressure relation can be observed in all simulation results ($\Delta P_{cap} > \Delta P_{pl} > \Delta P_{ra}$) during the mechanical inspiration. Figure 15, plot (4) bottom depicts the change of left and right ventricular volumes during VCV. As expected by Jardin, an increase in left ventricular and decrease in right ventricular volumes can be quantitatively modeled. Note that it was not able to measure these volumes during Jardin's experiment.

Second case is a beat-to-beat analysis on 13 ventilated patients published in the same paper of Jardin et al. [8], which focused on the change in systemic and pulmonary arterial pressure during ventilated inhalation. Figure 16 (1) depicts the mean aortic and pulmonary arterial pressure in systole and diastole of these 13 patients. Jardin divided the 9 heart beats into three different respiratory phase: exhalation (beat 1-3), preinspiration (beat 4-6), and lung inflation (beat 7-9). During the last phase, he observed an increase in systemic arterial pressure, where systole is greater than diastole. The pulmonary arterial pressure also increased but exhibited an opposite change, where diastole is greater than systole. PCW increased slightly more than esophageal pressure. By applying the airway pressure on the model input, all these behaviors can be reproduced in simulation results (Fig. 16 (2)). The changes in systole-diastole gradient in systemic and pulmonary arterial pressure before and during an inhalation ($\Delta P_{sa,1} < \Delta P_{sa,2}$ and $\Delta P_{pa,1} > \Delta P_{pa,2}$) can be reproduced in the simulation.

3.2.3. Stroke volume during spontaneous breathing and positive-pressure ventilation

In this part, we compare cardiopulmonary dynamics between spontaneous breathing and positive-pressure ventilation. As reference, the experimental data published in [66], reviewed in [2], were reproduced and depicted in

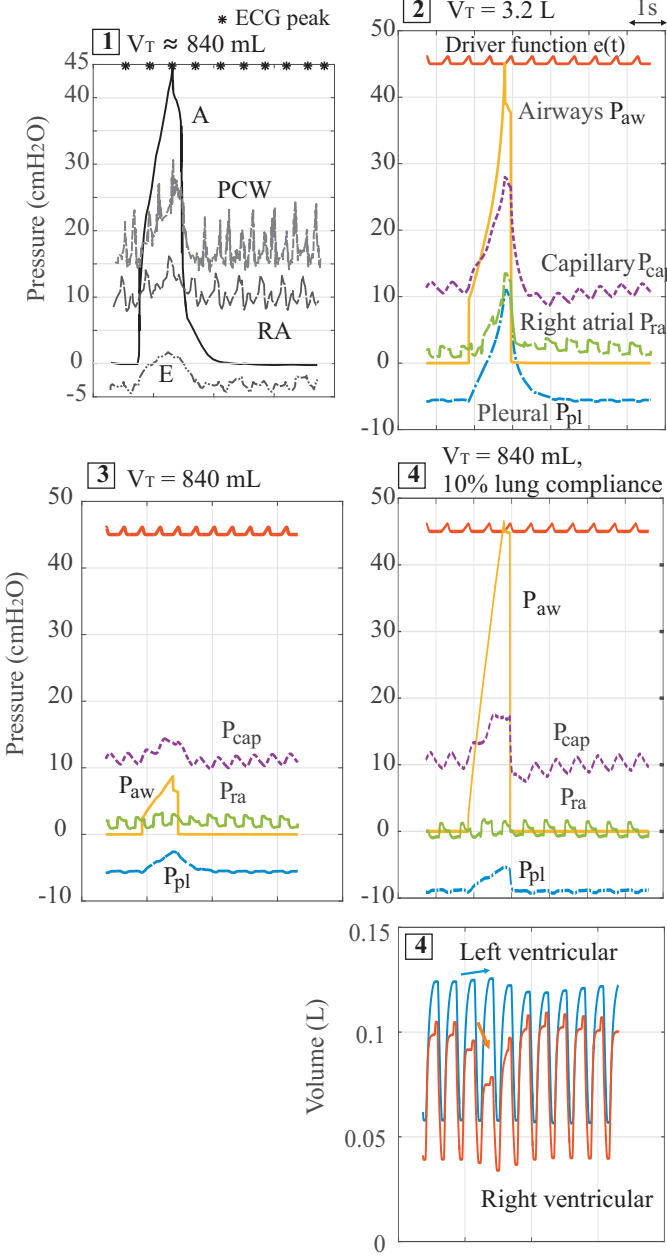


Figure 15: Pulmonary and cardiovascular pressures in patients under volume-controlled ventilation (VCV). (1): ECG and pressures of a patient under volumecontrolled ventilation. Data reproduced from [8]. PCW: pulmonary capillary wedge pressure, RA: right atrial pressure, A: airway pressure, E: esophageal pressure. During an inspiration, airway pressure increase to 30 mmHg. (2,3,4): simulative results with the model: driver function $e(t)$, pulmonary capillary, airway, right atrial and pleural pressure. (2) $V_T = 3.2$ L (3) $V_T = 3.2$ L volume. (4) $V_T = 3.2$ L and reduction of lung compliance by 90%. (4 bottom) Left and right ventricular volume for simulation (4).

Fig. 19. In anesthetized, intact canines, the authors found differential effects of negative (spontaneous inspiration) and positive (positive-pressure inspiration) changes in the intra-thoracic pressure on cardiovascular dynamics. The right ventricular SV rises with positive-pressure inspiration and falls with spontaneous inhalation, while the left ventricular SV behaved inversely with delay. For comparison, experimented and simulated airway and pleural pressures, as well as left and right ventricular SV are depicted in Fig. 19. Of the same simulation, aortic, left and right ventricular pressures, left and right atrial and ventricular volumes, venous return and cardiac output are presented in Fig 17. The pressure-controlled ventilation was set between 0 and 10 cmH₂O. Stroke volume (SV) was calculated by integrating stroke flows over a heart beat.

Simulation results are comparable with animal data. The left and right ventricular SV is smaller in canine (15 - 18 mL) comparing to those of a human (50 - 60 mL) due to the size of the animal. During spontaneous inspiration, venous return reached its maximum (approx. 0.8L/s in simulation) and left ventricular volume increased. During a ventilated inspiration, the process was inverse. In simulation, P_{alv} increased from 0 cmH₂O to 10 cmH₂O, which caused a fall in right ventricular pressure of 9.52 mmHg, a fall in right ventricular SV of 26.6 mL, and a rise in the average aortic pressure of approx. 5 mmHg. Right

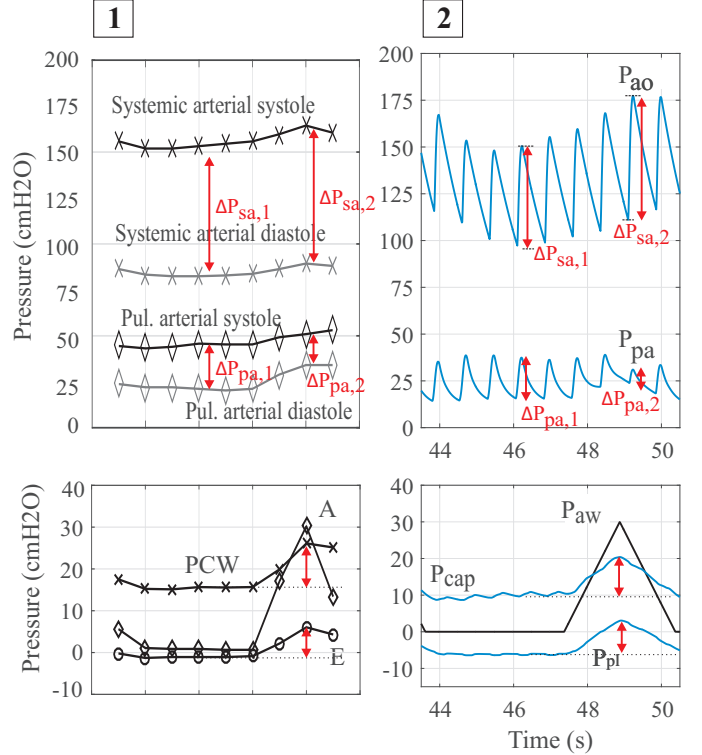


Figure 16: Aortic, pulmonary arterial and capillary pressure during a ventilation cycle. (1) Clinical data, reproduced from [8]. (2) Simulative results. The plots include aortic, pulmonary arterial, pulmonary capillary, airway and pleural pressures. Observation: $\Delta P_{sa,1} < \Delta P_{sa,2}$ and $\Delta P_{pa,1} > \Delta P_{pa,2}$.

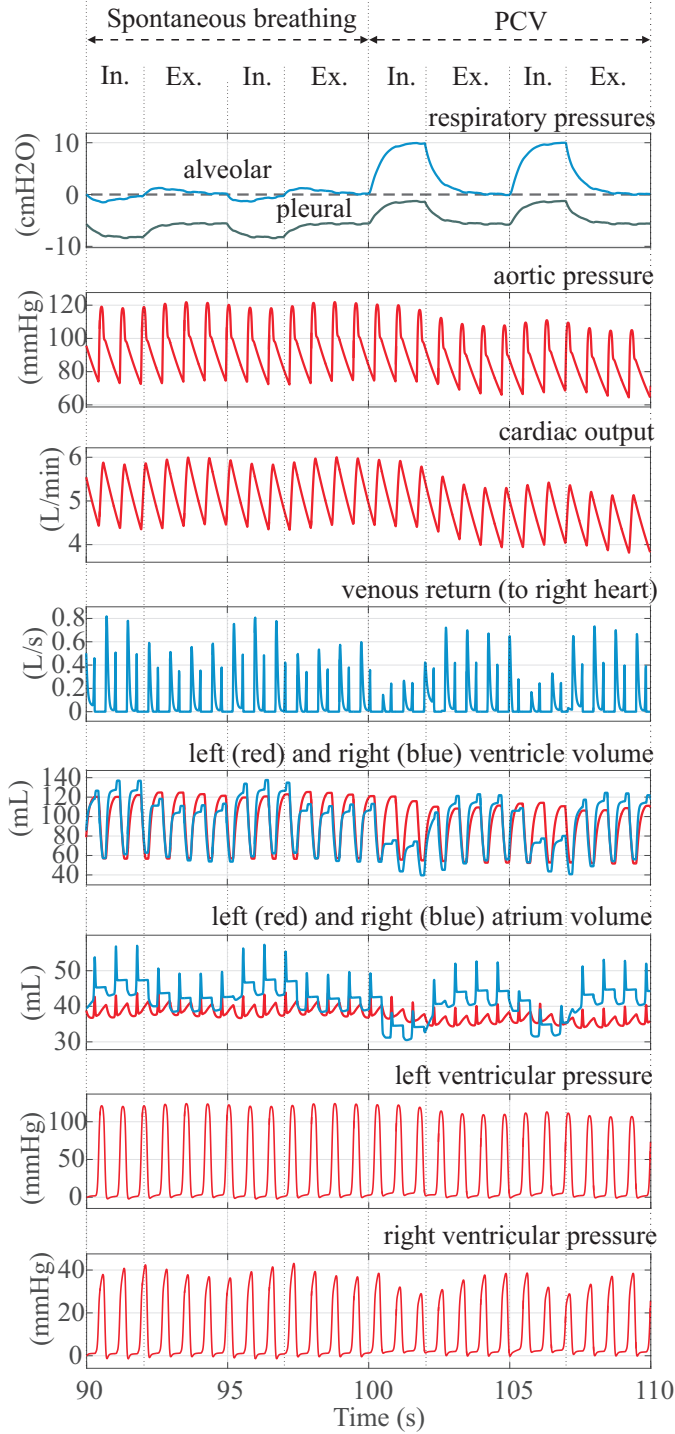


Figure 17: Influence of the respiration on pleural pressure, venous return, ventricular volumes and aortic pressure. Model behaviors correspond with animal experiments reported in [2]

ventricular SV decreased during the first heart beats after the start of inspiration, then rose slightly to a higher value after two heart beats. Left ventricular SV increased during the first heart beats and then fell to a value smaller than its start value. CPIs which are observed in animal experiments can be demonstrated by the model.

Next, we analyzed a schematic diagram to study CPIs

during mechanical ventilation published in [1]. According to the authors, on the one hand, an increase in airway pressure leads to a rise in transpulmonary pressure (TPP), an increase in pulmonary vascular resistance, and an increase in right ventricular afterload. On the other hand, a higher lung volume causes changes in ITP, which reduces venous return and right ventricular preload. Both result in a reduction of right ventricular, and then left ventricular SV (see Fig. 18). We drawn simulation results (at PIP = 10 and PEEP = 0 cmH₂O) to the diagram. The preload was presented by end-diastolic ventricular volume, the afterload by the arterial pressure. Simulation results correspond to the observation of Cherpanath, with an exception of a variable right ventricular afterload. Simulation results support the hypothesis that changes in left and right ventricular SV are primarily caused by the change in venous return due to the rise in ITP, and less by the change in right ventricular afterload, as reported in other literature [3, 2].

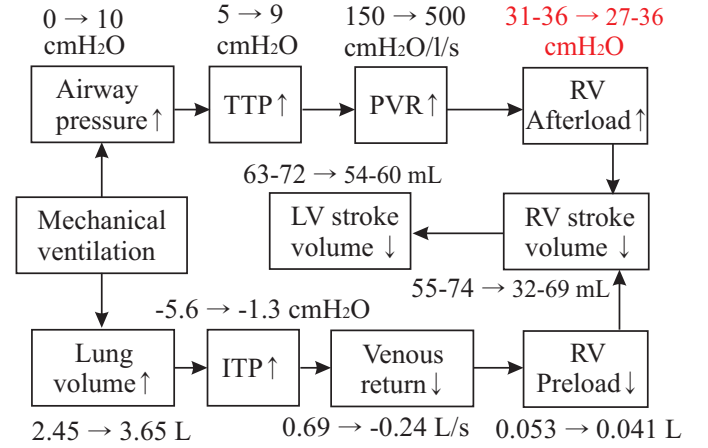


Figure 18: Effect of mechanical ventilation of right and left ventricular stroke volume. Schema adapted from [1]. Simulation results with pressure-controlled ventilation at PIP=10 cmH₂O. TPP: transpulmonary pressure; PVR: pulmonary vascular resistance; ITP: intra-Åsthoracic pressure

3.2.4. Effect of PEEP on CPIs

The effect of PEEP on CPIs can not be neglected during the choice of ventilation settings. Scharf et al. [67] reported a correlation between PEEP and pleural, transpulmonary, pulmonary arterial, and right atrial pressures in anesthetized Mongrel dogs (22 – 25 kg). They were under VCV ($V_T = 300 - 350$ mL (12 – 14 mL/kg)) with different PEEP (measured) at 0.6, 4.3, 7.7, 11.4, and 16.4 cmH₂O. Figure 20 compares the experimental results from [67] and a simulation with VCV. Tidal volume was set to 12.7 mL/kg V_T (950 mL for a 75 kg healthy human). Two data sets correlate with each other. An increase in lung volume, as well as in transpulmonary, pleural, pulmonary arterial, and right atrial pressures can be found in two results. The transpulmonary and pulmonary arterial pressures are slightly higher in animal data than in simulation.

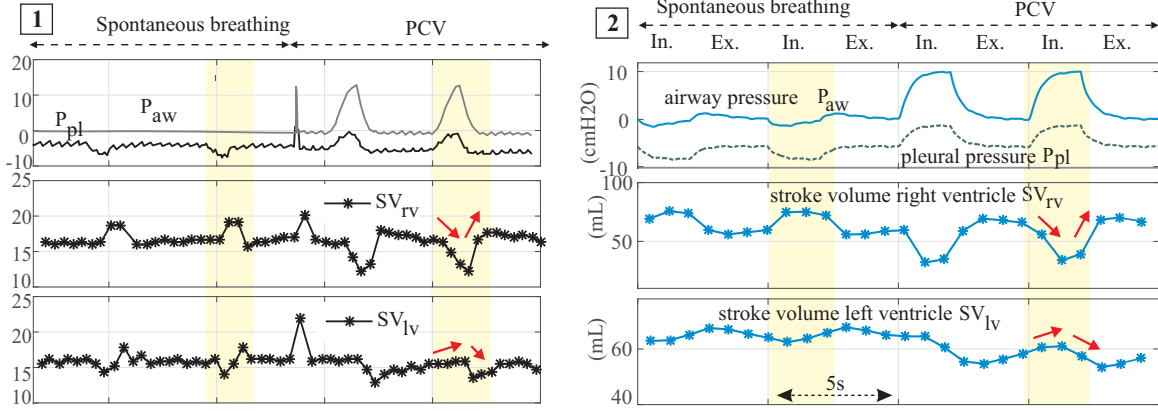


Figure 19: Cardiopulmonary interactions during spontaneous breathing and mechanical ventilation. (1) cardiopulmonary interactions observed in animal experiment, reproduced from [2, 66]. (2): model simulation results.

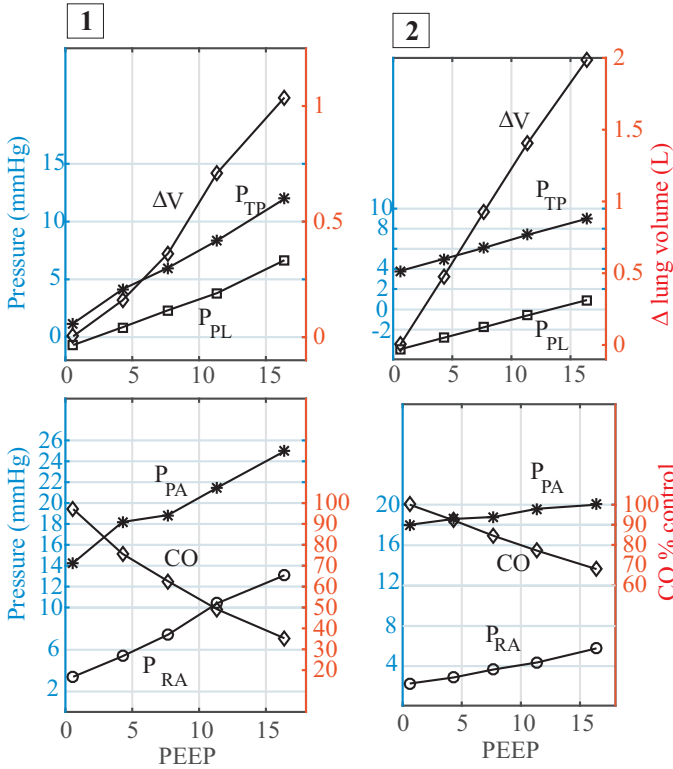


Figure 20: Effect of PEEP on lung volume, cardiac output (CO), as well as transpulmonary (TP), pleural (PL), pulmonary arterial (PA), and right atrial (RA) pressures during volume-controlled ventilation. (1) Experimental data in Mongrel dogs, data reproduced from [67], (2) Simulation results with $V_T = 12.7$ mL/kg

3.2.5. Heart failure and pulmonary congestion

The model can be used to investigate CPIs during pathological conditions. As an example, the model behavior under left heart failure (systolic dysfunction) and pulmonary congestion is shown. A left heart systolic dysfunction occurs if left ventricular stroke volume falls under 35 – 40% of the normal value [68]. This results in a blood volume shift from systemic to pulmonary circulation and an increase of pulmonary blood pressures (congestion). Left heart systolic dysfunction was simulated by reducing the left ventricular systolic elastance $E_{es,lvf}$ from eq. 2 to 50% and 20% of the original value. Figure 21 top left panel displays the PV-loops of the left ventricle at reduced elastances. At $E_{es,lvf} = 20\%$, left ventricular stroke volume fell to 42.2 mL (57% of the normal value), cardiac output to 3.3 L, and aortic pressure to 70.9/45.5 mmHg. Blood volume shift was simulated as well: systemic blood volume decreased to 2.78 L, while pulmonary venous and capillary blood volume rose to 365 mL and 285 mL, respectively (Fig. 21 top right panel). Pulmonary blood pressures increased, especially in the venous part (Fig. 21, bottom left panel). This increase indicates a possible development of pulmonary congestion [39]. Fig. 21 bottom right panel depicts the change of gas volume in the lungs caused by changes in intra-thoracic pressure due to left ventricular systolic dysfunction. While tidal volume remains unchanged, FRC reduced slightly by approx. 100 mL during left heart dysfunction.

4. Discussion

We have introduced a comprehensive model of cardiopulmonary interactions. The lumped-element model was implemented in the object-oriented language Simscape, in which the system equations are presented by physical blocks and connections. The model includes more than 30 elements which correspond to the same number of physiological functional components of the cardiopulmonary system. Simulation speed was found to be high

While cardiac output falls to 35% in dogs at a tidal volume of 300 – 350 mL, the model predicts a reduction of cardiac output to 65%. Note that we used the original parameter set for this simulation. An adaption of parameters based on parameter estimation would results in a better fit between model and data, but is not the objective of this paper.

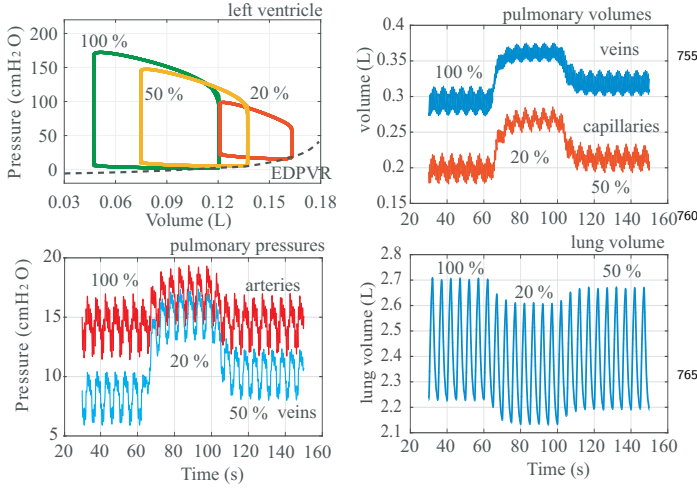


Figure 21: Simulation of a left heart failure by reducing E_{es} to 50% and 20% of the normal values (systolic dysfunction). Top left panel: PV-loops of left ventricle during systolic dysfunction. EDPVR = 770 end-diastolic pressure volume relationship. Other panels: changes in pulmonary pressure and volumes, and in lung volume during left heart failure. A congestion of pulmonary blood and a slightly fall in lung volume can be observed. Second 30 to 60: $E_{es} = 100\%$. Second 70 to 100: $E_{es} = 20\%$. Second 110 to 150: $E_{es} = 50\%$.

enough (30 times faster than real time on a PC with Intel Core i7-4770 CPU) for possible real-time applications.

Further comparisons between causal modeling (text-based, signal-oriented) and acausal modeling (object-oriented OOML) are discussed elsewhere [28, 69]. OOML has the main advantage that model balance equations are included in the graphical implementation of the model structure. Thus, while a large number of mathematical equations do not need to be explicitly implemented, 785 OOML also captures the essence of reality. Model components become more legible in OOML, which simplifies model extension and testing [69].

The cardiovascular system was developed based on the model of Smith et al. [32, 31] with the extension of atria-790 and non-linear characteristics of the veins and lung capillaries. Nonlinear PV relationships were included to give the model a higher robustness against parameter uncertainties, especially at boundary conditions such the collapse of the capillaries or veins. Some of the parameters 795 show a significant difference among physiological studies. For example, estimation of venous blood volume and compliance is difficult and differs between studies [37, 70]. Also, whereas aging increases a vessel's passive stiffness and thereby reduces compliance, the hormonal or neural 800 regulation additionally alters this stiffness by activating vascular smooth muscle [39, 40]. Therefore, it is important to note that our versatile model presents just one of many possibilities to simulate the cardiovascular interactions.

To our knowledge, our respiratory model is the first-805 object-oriented model to focus on non-linear functionality of lung compartments and succeeds in reproducing the static and dynamic behaviors of lung mechanics. Further-

more, the connection between the respiratory and hemodynamic system is the most complex published so far. The RS was divided into different compartments corresponding to their physiological and physical functions. Simulation results have demonstrated the accuracy of the model compared to the literature, during both spontaneous breathing and mechanical ventilation. Saturated behaviors of the system, such as over-stretching, could be simulated due to the implementation of non-linearities. Negative pleural and interstitium dynamics could also be adequately demonstrated. Overall, the model provides physiologically stable results for CPIs which could be directly compared with clinical and animal data from [8, 10, 2, 67].

Model limitation. Some factors have not been considered in the respiratory model. First, our compartmentalization is functional rather fragmentary, i.e. components such as nasal cavity, mouth, trachea, bronchial were not considered separately. Second, we neglected the inertance of gas and tissue, which does not affect lung dynamics during spontaneous breathing, but does have a strong influence during high frequency ventilation and oscillometry [71, 72, 73, 74]. Third, the inhomogeneity between left and right lungs [20], as well as between different lung layers [75] have also not yet been considered. Fourth, our modeling approach of the alveolar opening remains a simplification, since the hysteresis of the alveolar compartment during recruitment maneuvers [50] has not been considered in the model.

Moreover, our model does not include the gas exchange component, which would affect the hemodynamics regarding hypoxic pulmonary vasoconstriction or control of breathing and heart rate via central and peripheral chemoreceptor. Hypoxic pulmonary vasoconstriction in the lung is the mechanism underlying ventilation/perfusion matching to distribute blood flow regionally and increase the efficiency of gas exchange. Current models in literature use signal-based implementation for this component. It should be noted that the cardiac and respiratory regulation have not been included in the model. The model, in its current form, is almost completely passive. This means that all of the components (excluding the driver function of heart activity and the respiratory muscles) are passive elements which are described only by their physiological characteristics. However, simulation results have demonstrated the model's performance in studying CPIs. The model suggests that the passive intrathoracic pressure as mechanical coupling between the cardiovascular and respiratory system play an important role in CPIs and cannot be ignored when considering CPIs during PEEP trials.

Model potential use. This paper focus on the development and validation of a cardiopulmonary model for a healthy human, hence, does not include the modeling pathologies. However, as in the current form, the model can be extended for specific diseased conditions. As examples, left

or right heart failure can be induced by reducing ventricular systolic elastance, and a respiratory obstruction such as asthma or COPD can be modeled by increasing the peripheral resistance or reducing the bronchial compliance. More complex diseases such as cardiogenic edema, cardiac tamponade, ventilator-induced lung diseases, or acute respiratory distress syndrome require adequate model extensions.

Moreover, the model can be used as a simulator in a user-interactive software tool for educational and training purposes. In the future, bed-side model-based monitoring may be applied for personal health care, due to the development of an increasing number of sensor technologies to measure vital parameters. Also, a computational model (in combination with online parameter estimation) may provide clinicians with important information to support clinical diagnosis and treatment.

All simulation data reported in this paper are available from the corresponding author upon request. Further simulation data for specific testing purpose can be generated and provided by the authors upon reasonable request. The authors reserve the copyright of the software.

5. Conclusion

A comprehensive model of cardiopulmonary interactions implemented in the object-oriented language Matlab Simscape has been presented. The model includes the cardiovascular and respiratory systems with CPIs via intrathoracic and interstitial pressures. Baseline simulation and simulation during mechanical ventilation can be directly compared with animal and clinical data in literature.

6. Acknowledgment

This project is a part of the academic-industry cooperation between Philips Chair of Medical Information Technology, Helmholtz-Institute for Biomedical Engineering, RWTH Aachen University and Philips Technologie GmbH Innovative Technologies, Aachen, Germany. Chuong Ngo gratefully acknowledges the financial support of Philips Technologie GmbH Innovative Technologies, Aachen, Germany.

References

- [1] T. Cherpanath, W. K. Lagrand, M. Schultz, A. Groeneveld, Cardiopulmonary interactions during mechanical ventilation in critically ill patients, *Netherlands heart journal : monthly journal of the Netherlands Society of Cardiology and the Netherlands Heart Foundation* 21 (4) (2013) 166–172. doi:10.1007/s12471-013-0383-1.
- [2] H. Gomez, M. Pinsky, Effect of mechanical ventilation on heart-lung interactions, in: *Principles and Practice of Mechanical Ventilation*, McGraw-Hill New York, 2013, pp. 821–849.
- [3] M. Pinsky, The hemodynamic consequences of mechanical ventilation: an evolving story, *Intensive care medicine* 23 (5) (1997) 493–503.
- [4] M. Pinsky, Cardiovascular issues in respiratory care, *CHEST Journal* 128 (5 Suppl 2) (2005) 592S–597S.
- [5] T. Luecke, P. Pelosi, Clinical review: Positive end-expiratory pressure and cardiac output, *Critical care (London, England)* 9 (6) (2005) 607–621.
- [6] R. Bronicki, N. Anas, Cardiopulmonary interaction, *Pediatric Critical Care Medicine* 10 (3) (2009) 313–322.
- [7] R. Wise, J. Robotham, W. Summer, Effects of spontaneous ventilation on the circulation, *Lung* 159 (1) (1981) 175–186.
- [8] F. Jardin, J. Farcot, P. Gueret, J. Prost, Y. Ozier, J. Bourdarias, Cyclic changes in arterial pulse during respiratory support, *Circulation* 68 (2) (1983) 266–274.
- [9] J. F. Jallon, E. Abdulhay, P. Calabrese, P. Baconnier, P.-Y. Gumery, A model of mechanical interactions between heart and lungs, *Philosophical Transactions of the Royal Society of London A: Mathematical, Physical and Engineering Sciences* 367 (1908) (2009) 4741–4757.
- [10] J. Robotham, J. Rabson, S. Permutt, B. Bromberger-Barnea, Left ventricular hemodynamics during respiration, *Journal of Applied Physiology* 47 (6) (1979) 1295–1303.
- [11] J. Robotham, W. Mintzner, A model of the effects of respiration on left ventricular performance, *Journal of Applied Physiology* 46 (3) (1979) 411–418.
- [12] F. Grodins, Integrative cardiovascular physiology: a mathematical synthesis of cardiac and blood vessel hemodynamics, *Quarterly Review of Biology* (1959) 93–116.
- [13] E. Shim, J. Sah, C. Youn, Mathematical modeling of cardiovascular system dynamics using a lumped parameter method, *The Japanese journal of physiology* 54 (6) (2004) 545–553.
- [14] O. Barnea, Open source programming of cardiovascular pressure-flow dynamics using simpower toolbox in matlab and simulink, *The Open Pacing, Electrophysiology & Therapy Journal* 3 (2010) 55–59.
- [15] J. Olansen, J. Clark, D. Khoury, F. Ghorbel, A. Bidani, A closed-loop model of the canine cardiovascular system that includes ventricular interaction, *Computers and biomedical research, an international journal* 33 (4) (2000) 260–295. doi:10.1006/cbmr.2000.1543.
- [16] L. Cheng, O. Ivanova, H. Fan, M. Khoo, An integrative model of respiratory and cardiovascular control in sleep-disordered breathing, *Respiratory physiology & neurobiology* 174 (1-2) (2010) 4–28. doi:10.1016/j.resp.2010.06.001.
- [17] S. Heinke, C. Pereira, S. Leonhardt, M. Walter, Modeling a healthy and a person with heart failure conditions using the object-oriented modeling environment dymola, *Medical & Biological Engineering & Computing* 53 (10) (2015) 1049–1068.
- [18] A. Brunberg, S. Heinke, J. Spillner, R. Autschbach, D. Abel, S. Leonhardt, Modeling and simulation of the cardiovascular system: a review of applications, methods, and potentials/modellierung und simulation des herz-kreislauf-systems: ein überblick zu anwendungen, methoden und perspektiven, *Biomedical Engineering* 54 (5) (2009) 233–244.
- [19] T. Heldt, E. B. Shim, R. D. Kamm, R. G. Mark, Computational modeling of cardiovascular response to orthostatic stress, *Journal of applied physiology* 92 (3) (2002) 1239–1254.
- [20] A. Otis, C. McKerrow, R. Bartlett, J. Mead, M. McIlroy, N. Selverstone, E. Radford, Mechanical factors in distribution of pulmonary ventilation, *Journal of Applied Physiology* 8 (4) (1956) 427–443.
- [21] J. Mead, Mechanical properties of lungs, *The American Physiological Society* 41 (2) (1961) 281–330.
- [22] V. Rideout, Mathematical and computer modeling of physiological systems, Prentice Hall advanced reference series. Physical and life sciences, Prentice Hall, Englewood Cliffs and N.J., 1991.
- [23] A. Albanese, L. Cheng, M. Ursino, N. Chbat, An integrated mathematical model of the human cardiopulmonary system: model development, *American journal of physiology. Heart and circulatory physiology* 310 (7) (2016) H899–921. doi:10.1152/ajpheart.00230.2014.
- [24] S. Leonhardt, S. Böhm, B. Lachmann, Optimierung der beatmung beim akuten lungenversagen durch identifikation physiologischer Parameter, *Medical Engineering & Physics* 36 (2014) 1049–1068.

1075 increasing airway pressure in the dog, American Journal of
Physiology-Heart and Circulatory Physiology 232 (1) (1977)
H35–H43.

[68] A. Hummel, K. Empen, M. DÄürr, S. Felix, Akute und
akut dekompenzierte chronische herzsuffizienz, Deutsches
ÄDrzteblatt (17) (2015) 298–310.

1080 [69] J. Kofránek, M. Mateják, P. Privitzer, M. Tribula, Causal or
acausal modeling: labour for humans or labour for machines,
Technical Computing Prague (2008) 1–16.

[70] P. Johnson, K. Hanson, Relation between venous pressure and
blood volume in the intestine, American Journal of Physiology
204 (1963) 31–34.

1085 [71] J. Bates, C. Irvin, R. Farré, Z. Hantos, Oscillation mechanics of
the respiratory system, Comprehensive Physiology 1 (3) (2011)
1233.

[72] J. Bates, Lung mechanics: an inverse modeling approach, Cam-
bridge University Press, 2009.

1090 [73] C. Ngo, A. Kube, K. Krüger, T. Vollmer, S. Winter, S. Leon-
hardt, B. Misgeld, Identification of respiratory parameters in fre-
quency and time domain with forced oscillation technique, in:
The International Federation of Automatic Control (Ed.), The
9th IFAC Symposium on Biological and Medical Systems, 2015,
pp. 177–182.

1095 [74] C. Ngo, S. Spagnesi, C. Munoz, S. Lehmann, T. Vollmer, B. Mis-
geld, S. Leonhardt, Assessing regional lung mechanics by combin-
ing electrical impedance tomography and forced oscillation
technique, Biomedical Engineering/Biomedizinische Technik.

1100 [75] J. West, Respiratory physiology: the essentials, Lippincott
Williams & Wilkins, 2012.

Table A.11: List of indexes.

tm	transmural
es	end-systolic
ed	end-diastolic
ra	right atrial
la	left atrial
rv	right ventricular
lv	left ventricular
ao	aortic
sa	systemic arterial
sv	systemic venous
pv	pulmonary venous
pa	pulmonary atrial
cap	pulmonary capillary
pvc	pulmonary venous capillary
tp	transpulmonary
alv	alveolar
int	interstitial
pl	pleural
mus	respiratory muscular
col	collapsible airway
cw	chest wall
L	lung
T	tidal (volume)

AppendixA. Abbreviations and list of indexes

Table A.10: Abbreviations

CPIs	Cardiopulmonary interactions
CPS	Cardiopulmonary system
CVS	Cardiovascular system
ECG	Electrocardiogram
EDPVR	End-diastolic pressure volume relationship
ESPVR	End-systolic pressure volume relationship
FRC	Functional residual capacity
ITP	intra-thoracic pressure
OOML	Object-oriented modeling language
PEEP	Positive end-expiratory pressure
PCV	Pressure-controlled ventilation
PCW	Pulmonary capillary wedge pressure
PV	Pressure-volume
PVR	Pulmonary vascular resistance
RS	Respiratory system
SV	Stroke volume
TPR	Total peripheral resistance
TPP	Transpulmonary pressure
VCV	Volume-controlled ventilation

AppendixB. Heart components

Driver functions of atria, ventricles and septum:

$$\begin{aligned}
 e_{la,ra}(t) &= A_a \cdot e^{-\frac{0.5}{B_a^2} \cdot \left(\frac{HR}{80}\right)^2 \cdot (t - C_a \cdot \frac{80}{HR})^2} \\
 e_{lvf,rvf}(t) &= \sum_{i=1}^4 A_i \cdot e^{-\frac{0.5}{B_i^2} \cdot \left(\frac{HR}{80}\right)^2 \cdot (t - C_i \cdot \frac{80}{HR})^2} + D \\
 e_{sept}(t) &= e_{lvf}(t)
 \end{aligned} \tag{B.1}$$

1105 A , B , and C are the Gaussian magnitude, width, delay, respectively [15]. HR is the heart rate. D is a baseline/offset which prevents the ventricular pressure from reaching negative values. D is equal 0.02 for the left and 0.07 for the right ventricle.

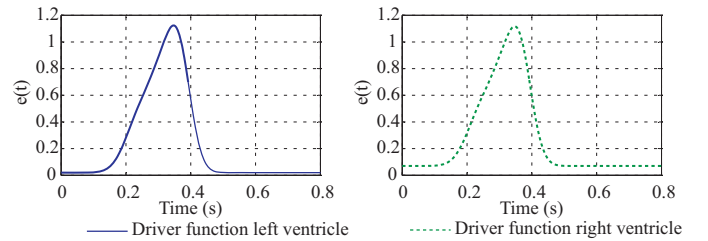


Figure B.22: Left and right ventricular driver functions.

1110

Param.	Units	$i = 1$	$i = 2$	$i = 3$	$i = 4$
$A_{v,i}$	–	0.43	0.36	0.5	0.55
$B_{v,i}$	s	0.045	0.035	0.037	0.036
$C_{v,i}$	s	0.175	0.23	0.275	0.3
A_a	–	0.9	–	–	–
B_a	s	0.018	–	–	–
C_a	s	0.065	–	–	–

ESPVR and EDPVR of four heart chambers and septum:

$$P_{es} = E_{es} \cdot (V - V_d)$$

$$P_{ed} = P_0 \cdot (e^{\lambda(V-V_0)} - 1)$$

$$P(V, t) = e(t) \cdot P_{es}(V) + (1 - e(t)) \cdot P_{ed}(V)$$

Pressure-volume relationship of the pericardium:

$$P_{pcd}(t) = P_{0,pcd}(e^{\lambda_{pcd}(V_{pcd}(t)-V_{0,pcd})} - 1)$$

Param.	P_0	V_0	V_d	λ	E_{es}
Units	cmH ₂ O	mL	mL	L ⁻¹	cmH ₂ O L ⁻¹
la	1.1236	0	20	60	294.27
ra	1.1236	0	20	50	217.53
lvf	0.0926	20	15	33	3573.7
rvf	0.211	20	5	23	895.5
sept.	1.5096	2	2	435	66303
peri.	0.068	260	–	30	–

Volume balance equations:

$$V_{lvf} = V_{lv} - V_{spt}$$

$$V_{rvf} = V_{rv} + V_{spt}$$

$$V_{lv} = V_{lvf} + V_{spt}$$

$$V_{rv} = V_{rvf} - V_{spt}$$

$$V_{pcd}(t) = V_{la}(t) + V_{lv}(t) + V_{ra}(t) + V_{rv}(t)$$

Heart valves

	Transmitting resistance
Tricuspid	4.0789
Pulmonary	2.7191
Mitral	13.5955
Aortic	6.7977

Table B.12: Heart valve transmitting resistances, from [31]. Values given in [cmH₂O s L⁻¹].

AppendixC. Pulmonary and systemic circulation

AppendixC.1. Veins

Normal veins:

$$V = \frac{1}{\lambda} \cdot \log(P_{tm} + P_0) + V_0 \quad (C.1)$$

1115

Collapsed veins:

if $V \leq V_{clp}$

$$V = 0.2 \cdot V_{clp} \cdot \tanh\left(\frac{5}{V_{clp} \cdot \lambda \cdot (P_{clp} + P_0)} \cdot (P - P_{clp})\right) + V_{clp}$$

$$P_{clp} = e^{\lambda(V_{clp} - V_0)} - P_0$$

where V_{clp} is a threshold volume of collapsed veins.

Param.	P_0	V_0	V_{clp}	λ
Units	cmH ₂ O	L	L	L ⁻¹
Syst. veins	6.328	1.8456	1.25	1.8361
Pulm. veins	-3.567	0.0895	0.0625	10

1120

AppendixC.2. Pulmonary capillaries

Pulmonary capillaries compliance:

$$V = V_0 + \frac{1}{\lambda} \cdot \tanh(c \cdot P_{tm} + P_0) \quad (C.2)$$

Pulmonary capillaries resistance:

$$R = R_1 \cdot \frac{(V_1 - 0.9V_{min})^2}{(V_t - 0.9V_{min})^2} \quad (C.3)$$

Parameters of the pulmonary capillaries are given in Table 1. The systemic capillaries are included in the systemic arteries.

1125 AppendixC.3. Arteries

The pressure-volume characteristics of pulmonary and systemic arteries:

$$V - V_d = P_{tm} \cdot C \quad (C.4)$$

Param.	C	V_d
Units	L/cmH ₂ O	L
Syst. arteries	0.0011	0.6
Pulm. arteries	0.0022	0.1

AppendixD. Respiratory muscles

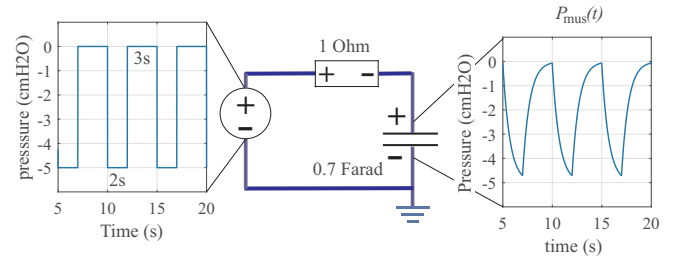


Figure D.23: The respiratory muscles P_{mus} during spontaneous breathing, generated by a pulse generator and a RC network.

Figure D.23 illustrates the implementation for P_{mus} . The signal was generated by means of a periodic rectangular pulse generator and a resistance-compliance (RC) network (Voigt model of visco-elastic behavior).

1130

AppendixE. Exemplary Simscape code of a model component

The following Simscape code presents the non-linear resistance of the collapsible airways (see eq.7). A component belongs to a domain (in this case electrical.branch) and contains parameters, inputs, outputs, and equations. It should be distinguished between algebraic (with '=') and physical equations (with '==').

```
1135 component R_vessel < foundation.electrical.branch
% non-linear collapsible resistance
    R1      = { 1, 'Ohm' };    % R1
    V1      = { 0.1, 'A*s' };  % V1
    Vmin    = { 0.05, 'A*s' }; % Vmin
1145 end
inputs
    Vol     = { 1, 'A*s' };    % Volume
end
outputs
1150 Rout     = { 1, 'Ohm' };    % R_out
end
equations
    let
        R      = R1*(V1-0.9*Vmin)/(Vol-0.9*Vmin);
1155    in
        v      == R*i;
        Rout   == R;
    end
end
1160 end
```